THE ASTROPHYSICAL JOURNAL, 419:12–29, 1993 December 10

THE ANALYSIS OF GRAVITATIONAL LENS SURVEYS. II. MAXIMUM LIKELIHOOD MODELS AND SINGULAR POTENTIALS

CHRISTOPHER S. KOCHANEK[1]
Harvard-Smithsonian Center for Astrophysics, 60 Garden Street, Cambridge, MA 02138
Received 1993 January 8; accepted 1993 June 21

ABSTRACT

We do a maximum likelihood analysis of three optical surveys for gravitational lenses. The results are consistent with lensing by normal galaxies modeled as singular isothermal spheres with standard values for observational parameters, aside from the need to add a small amount of ellipticity to produce the observed four image lenses. We tested the model for variations in the number of galaxies, the velocity dispersions of galaxies, the distribution of galaxies, the relation between luminosity and velocity dispersion, the quasar apparent magnitude number counts, and the mean magnification produced by the lenses. No variation we examined significantly improved the likelihoods over using the standard observational values, although there is weak evidence for differences in the magnification bias. The measured isothermal velocity dispersion of an L_* E/S0 galaxy is $\sigma_* = 245$ km s^{-1} with a 90% confidence interval of 210 km s^{-1} $\lesssim \sigma_* \lesssim$ 270 km s^{-1}, ignoring the lens 0957+561. This is consistent with the estimated range from dynamical studies of 183–248 km s^{-1}. The measured comoving density of galaxies or dark halos on this mass scale is $6.7 \times 10^{-3} h^3$ Mpc^{-3} with a 90% confidence interval from $2.0 \times 10^{-3} h^3$ Mpc^{-3} to $1.7 \times 10^{-3} h^3$ Mpc^{-3}. Depending on systematic assumptions about treating the lens 0957+561 and the contribution of spiral galaxies to lensing, the upper limit on the value of the cosmological constant can be as high as $\Omega_\Lambda \lesssim 0.8$ or as low as $\Omega_\Lambda \lesssim 0.45$. Doubling the sample size will reduce the confidence intervals to levels where contradictions with other observations may become apparent.

Subject headings: cosmology: observations — galaxies: distances and redshifts — galaxies: structure — gravitational lensing

1. INTRODUCTION

Several large surveys for gravitational lenses among bright quasars (Surdej et al. 1993; Crampton, McClure, & Fletcher 1992; Yee, Fillipenko, & Tang 1992; Bahcall et al. 1992; Maoz et al. 1992b, 1993a, b) and radio sources (Patnaik et al. 1992a; Burke, Lehàr, & Connor 1992) are now completed or approaching completion. The analysis of surveys has been primative, relying solely on a preexisting, fixed model of gravitational lens statistics and Poisson statistics to compare the fixed model to the observed incidence of lenses. The statistics are based on simple theoretical models popularized by Turner (1990) using the observed number counts of galaxies, Tully-Fisher/Faber-Jackson relations, and the simple singular isothermal sphere model for the lens galaxies. More realistic lens models with both core radii and ellipticity have been explored in detail by Blandford & Kochanek (1987), Kochanek & Blandford (1987), Kochanek (1991b), and Wallington & Narayan (1993).

We would like to use the statistics of lenses for three purposes: first, to constrain the cosmological model; second, to constrain the mass and structure of galaxies; and third, to make estimates of what further observations could contradict or improve the statistical model. The observables that can be used to constrain models are the incidence of lenses, which quasars are lenses, and the properties of the individual lenses such as image separation, flux ratios, morphology, and lens redshifts. Poisson statistics use little of the information provided by a large lens survey because reducing the problem to only the expected number of lenses throws away much of the information.

The first step in improving the statistical models of surveys is to use all the variable data from the gravitational lenses found in the surveys. The second step is to assume a minimum amount of a priori knowledge about masses and distributions of galaxies. The arguments for and against a particular cosmological model rest on the assumed value for galactic masses in the standard analysis of lens statistics. We can eliminate a major source of systematic uncertainties if we use the lensing phenomenon itself to determine both the masses of galaxies and the cosmological model self consistently. Wherever possible we explore the ability of the lens statistics to measure other assumed properties such as the Faber-Jackson (1976) relationship—often the results are only indicative because the lens surveys are still too small, but this will change as the size of the surveys increases. All these goals point toward a statistical model based on maximum likelihood techniques, in which the parameters of the statistical model are adjusted to maximize the likelihood of finding the observed sample. The likelihood function is chosen to incorporate all the available information on the properties of the survey, thus maximizing the sensitivity of the model. We then compare the predictions from the lens model to the standard observational estimates to see if there are any contradictions.

We use the simple SIS model to take advantage of its simplicity, but we use Monte Carlo techniques to determine whether we are justified in using the model. Once we have found the maximum likelihood estimates of the parameters for the lens model, we generate Monte Carlo observations of the same set of quasars using the true statistics of the SIS model. We then compare maximum

[1] Alfred P. Sloan Research Fellow.

likelihood models of the synthetic observations to those of the real observations to see if a more complicated model is needed to explain the observations.

This paper is the second in a series of papers on the statistical analysis of gravitational lens surveys. Paper I (Kochanek 1993b) focused on the issue of selection functions and ambiguous candidates in the optical surveys. This paper develops the statistical framework for performing the analysis of the optical quasar surveys, and applies these techniques using the singular isothermal sphere model of galaxies. In § 2 we discuss the basis for maximum likelihood models of lens statistics and contrast them with Poisson statistics. In § 3 we discuss the lens survey data we use in our analysis. In § 4 we discuss the statistical model used to analyze the surveys, which we apply in § 5. In § 6 we suggest how the statistics can be improved, and we summarize our results in § 7.

2. MAXIMUM LIKELIHOOD ANALYSIS OF LENS SURVEYS

All analyses of lens surveys to date have used Poisson statistics to evaluate the likelihood that the observed sample agrees with the expectations of lens theory. In the Poisson model, no weight is attached to which of the observed sample happens to be a lens—the only information used in the analysis is the number of lenses. Let the probability that quasar i is lensed be $p_i \ll 1$, where we have $i = 1 \ldots N$ quasars in the sample, of which N_L are observed to be gravitational lenses. The expected number of lenses in the sample is $\langle N_L \rangle = \sum_{i=1}^{N} p_i$ and the Poisson probability is simply

$$\begin{aligned} \ln P_{\rm tot} &= N_L \ln \langle N_L \rangle - \langle N_L \rangle - \ln N_L! \, , \\ &= -N\langle p_i \rangle + N_L \ln \langle p_i \rangle + \text{constant} \, , \end{aligned} \tag{2.1}$$

where $\langle p_i \rangle = \langle N_L \rangle / N$ is the average probability that a quasar is lensed. This expression gives no weight to which quasars were lensed or to the properties of the lensed images.

Let us now add the additional information that quasars $i = 1 \ldots N_U$ were unlensed, and quasars $j = 1 \ldots N_L$ were lensed. The likelihood function for the observation is $P_{\rm tot} = \prod_{i=1}^{N_U} (1 - p_i) \prod_{j=1}^{N_L} p_j$, which becomes

$$\ln P_{\rm tot} = -\sum_{i=1}^{N_U} p_i + \sum_{j=1}^{N_L} \ln p_j \tag{2.2}$$

under the assumption that $p_i \ll 1$. This expression is nearly identical to the Poisson result (eq. [2.1]) if the probability of being lensed is the same for all quasars ($p_i = \langle p_i \rangle$). This is not true for gravitational lenses, since the probabilities vary strongly with quasar redshift and magnitude. The likelihood function weights the results by the shape of the probability distributions, so it can differentiate between models that produce the same expected number of lenses using different shapes for the probability distribution. For example, it breaks the degeneracy between the cosmological model, which changes the probability distribution in quasar redshift, and additional magnification, which changes the probability distribution in lens magnitude.

This probability function still has trouble distinguishing between numbers of galaxies, galaxy masses, and cosmological models because it has no sensitivity to the mass of the lenses and it includes no information on the image morphology. Therefore we add a *configuration probability* p_{cj} to the likelihood function for each lens, which is the probability that the lens has some particular configuration. In particular we include the probability that the lens has the observed image separations. Thus our third likelihood function is

$$\ln P_{\rm tot} = -\sum_{i=1}^{N_U} p_i + \sum_{j=1}^{N_L} \ln p_j + \sum_{j=1}^{N_L} \ln p_{cj} \, , \tag{2.3}$$

where p_{cj} is the configuration probability. We treat the configuration probability separately because the number and type of extra data may vary from lens to lens.

Each of the likelihoods must be computed within the framework of a statistical model of the lenses and the survey selection effects. In the next sections we discuss the available data, the magnitude of selection effects in the data, and a series of statistical models. If we examine several lens surveys simultaneously, each survey has different selection functions based on its resolution and dynamic range, and hence the likelihoods p_i and p_{ci} will be different for each survey. If we combine surveys of different objects in one global optimization, we sum the logarithms of the likelihoods for the individual surveys, whereas if we combine surveys of the same objects we use the joint selection function of the two surveys.

3. AVAILABLE DATA ON LENSES

The largest homogeneous, published gravitational lens survey is the Snapshot Survey (Bahcall et al. 1992; Maoz et al. 1992b, 1993a, b) with 502 objects. Other surveys are Crampton et al. (1992) with 100 objects, Yee et al. (1993) with 108 objects and one known lens (Q1413+117), and ESO/Liège Survey (Surdej et al. 1993) with 188 objects and four lenses (PG1115+080, Q1413+117, 0142−100, and 1208−101). All these surveys selected high-redshift, high-luminosity quasars, and as a result there is considerable overlap between their samples. If we exclude the five lenses, there are 888 observations of 648 distinct quasars between the four surveys: 453 were observed by only one survey, 162 by two surveys, 22 by three surveys, and 11 by all four surveys. The Snapshot Survey examined 54 Crampton et al. (1992) objects, 52 Yee et al. (1992) objects, and 111 ESO/Liège Survey objects leaving 322 unduplicated objects. Crampton et al. (1992) examined 34 Yee et al. (1992) objects and 15 ESO/Liège Survey objects leaving 32 unduplicated objects. Yee et al. (1992) examined 28 ESO/Liège Survey objects leaving 35 unduplicated objects, and the ESO/Liège Survey has 64 unduplicated objects. Paper I gives an extensive discussion of the selection effects and reliability of the individual

surveys. We use the results of the Snapshot Survey, Crampton et al. (1992), and Yee et al. (1992) surveys in this analysis. The addition of the ESO/Liège Survey data would have a negligible effect since it includes only 64 new objects.

There are six lensed quasars in the combined sample: 0142−100, 0957+561, PG 1115+080, 1208+101, 1413+117, and 2237+0305. Of these lenses, only 1208+101 was "found" in the Snapshot Survey (Maoz et al. 1992a; Magain et al. 1992). The remaining lenses met the selection criterion of the Snapshot Survey and would have been observed if they were not protected by the rules governing *HST* observations. In testing statistical hypothesis the lens 2237+0305 must be removed from the sample because it is only in the quasar catalog because it is a lens—2237+0305 was found in a redshift survey of galaxies (Huchra et al. 1985) and the statistics of lenses in redshift surveys are different from that of lensing known quasars (Kochanek 1992b). We should bear in mind that 0957+561 (Young et al. 1980) is a composite lens consisting of a galaxy and a cluster so that the statistical model we apply may not be directly applicable. We shall include it in our analysis because we have not directly assumed our lenses consist only of isolated galaxies.

The largest surveys for gravitational lenses are not the optical surveys but the MG radio survey (Burke et al. 1992) and the Jodrell radio survey (Patnaik et al. 1992a, b, c). Unfortunately, we cannot use these surveys in estimating the absolute incidence of gravitational lenses because we do not have the full source lists, redshift distributions, and number-flux relations for the samples. Moreover, there are strong indications that the radio surveys are incomplete based on the distribution of image morphologies (Kochanek & Lawrence 1990). We can, however, include the configuration probabilities for the lenses these surveys have found if we can estimate the angular selection function of the surveys. The MG survey uses an outer limit for the best class of lens candidates of 10″.0 (Lehàr 1991) and is limited by the response of the VLA at small separations. Four of the MG lenses were found in the C-band survey, 2016+112 (b = 1″.9). 0414+053 (b = 1″.05), 1131+045 (b = 1″.05), and 1654+134 (b = 1″.0), and one has been found in the X-band survey 1549+304 (b = 0″.85). For the C-band survey we model the selection function as being uniform for critical radii from 0″.5 to 5″.0, and for the X-band survey we model the selection function as being uniform for critical radii from 0″.25 to 5″.0. We assume that the selection function for the observed radio lens morphologies is uniform over this angular range, not that the surveys are complete over this angular range. Similarly, the Jodrell survey has found three lenses, 1422+231 (b = 0″.65), 1938+666 (b = 0″.46), and 0218+356 (b = 0″.17), and we model the Jodrell selection function as being uniform for critical radii from 0″.1 to 5″.0.

The properties of the lenses are summarized in Table 1 and they are reviewed by Surdej et al. (1992), Burke et al. (1992), and Patnaik et al. (1992a). The primary information we can use about the lenses is their apparent magnitude, source redshift, image multiplicity, and image separation. We know both the source and lens redshifts for 0957+561, 0142−100, 1654+134, and 2016+112. We use a discretized version of the selection function because it allows the computations to use incomplete gamma functions rather than numerical integrals. The optical selection functions are given in Table 2. Arguably we are too conservative in setting the dynamic range of the survey at large image separations. However, as we argue in Paper I, there is little advantage from using higher dynamic ranges in lens surveys, so our conservatism has few statistical consequences.

4. MODELS USING SINGULAR ISOTHERMAL SPHERES

The likelihood analysis is best done by testing a particular hypothesis with a limited number of free parameters. Popular interest has focused on the variability between cosmological models (e.g., Turner 1990; Fukugita & Turner 1991; Krauss & White 1992; Kochanek 1992a, 1993a), so we should certainly include a range of cosmological models. The standard "null hypothesis" model of gravitational lens potentials is the singular isothermal sphere (SIS). We use the SIS model both for its analytic tractability and to test whether we can find any statistical reasons to reject it as a model by testing the best-fit SIS models against Monte Carlo simulations. We also try several tests to see if any modifications to the lens model improve the statistics. We use standard observational parameters for the number and distribution of galaxies and quasars and the relation between luminosity and velocity dispersions. In each case we test to see if the parameter estimates using lens statistics disagree with other observations.

TABLE 1

KNOWN LENSES IN THE SURVEYS

Name	Alternate	Source z_s	Lens z_L	m_V	N_{images}	$2b$[a]	Δm[b]	Selection
0142−100	UM673	2.72	0.5?	16.8	2	2″.2	2.1	S
0957+561	...	1.41	0.37	16.8	2	6″.2	0.3	S
PG1115+080	...	1.72	...	16.1	4	2″.2	0.1–2.1	S
1208+101	...	3.80	...	18.1	2	0″.48	1.5	S
1413+117	...	2.55	...	17.0	4	1″.2	0.1–0.6	S
2016+112	...	3.27	1.01	...	3	3″.8	...	MG-C
0414+053	...	2.63	...	...	4	2″.1	...	MG-C
1131+045	...	...	...	...	2	2″.1	...	MG-C
1654+134	...	1.75	0.25	...	R	2″.1	...	MG-C
1549+304	...	...	0.11	...	R	1″.7	...	MG-X
1422+231	...	3.62	...	...		1″.3	...	J
1938+666	...	...	...	...	4	0″.9	...	J
0218+356	...	...	...	...	2	0″.34	...	J

NOTES.—See Surdej et al. (1992a) for a review of lens observations.

[a] Twice the critical radius of the lens from Kochanek (1991a). This is roughly identical to the image separation.

[b] The maximum magnitude difference in the lens. For the four image lenses the minimum and maximum magnitude differences are given.

TABLE 2

Critical Radius Range	Magnitude Limit
A. Snapshot Survey Selection Function	
$0''.05 < b < 0''.10$	1.0
$0.10 < b < 0.15$	1.5
$0.15 < b < 0.20$	2.5
$0.20 < b < 0.25$	3.0
$0.25 < b < 3.50$	3.5
B. Crampton et al. (1992) Selection Function	
$0''.125 < b < 0''.150$	0.5
$0.150 < b < 0.175$	1.0
$0.175 < b < 0.200$	1.5
$0.200 < b < 0.225$	2.5
$0.225 < b < 0.250$	4.0
$0.250 < b < 3.000$	3.0
C. Yee et al. (1992) Selection Function	
$0''.125 < b < 0''.150$	0.5
$0.150 < b < 0.175$	1.0
$0.175 < b < 0.200$	1.5
$0.200 < b < 0.225$	2.5
$0.225 < b < 0.250$	4.0
$0.250 < b < 5.000$	5.0

4.1. *Observational Inputs*

The comoving number density of galaxies as a function of luminosity is modeled with a Schechter (1976) function,

$$\frac{dn}{dL} = \frac{n_*}{L_*}\left(\frac{L}{L_*}\right)^{\alpha} \exp\left(-\frac{L}{L_*}\right), \tag{4.1}$$

with the parameters set near the values of Efstathiou, Ellis, & Peterson (1988)

$$\alpha = -1.1 \pm 0.1, \qquad n_* = (1.6 \pm 0.3) \times 10^{-2} h^{-3}\ \mathrm{Mpc}^{-3}, \tag{4.2}$$

where the Hubble constant is $H_0 = 100h$ km s^{-1} Mpc^{-1}. We divide the galaxies into two classes. The early E/S0 class have comoving number density $n_e = (5.0 \pm 1.2) \times 10^{-3} h^3$ Mpc^{-3}, and the late S class have number density $n_s = (1.1 \pm 0.2) \times 10^{-2} h^3$ Mpc^{-3} using the fractional abundances of Postman & Geller (1984). The estimated errors on these variables (n_*, α, ...) are 1 σ errors. We use 90% confidence intervals to estimate errors, so the 1 σ errors quoted for the observational inputs should be roughly doubled when comparing them to our determinations from lens statistics.

To merge the galaxy counts with lens statistics we must assume a potential model for the galaxies and a relationship between luminosity and the dynamical variables of the potentials. We assume the mass distribution of a galaxy is that of the SIS. The SIS potential can successfully model all existing gravitational lenses with the addition of an elliptical perturbation (Kochanek 1991a). To use the SIS potential model we assume a power-law relation between galaxy luminosities L and one-dimensional velocity dispersions σ based on the form of the observed relationship between luminosities and central velocity dispersions (Faber & Jackson 1976) or rotation velocities (Tully & Fisher 1977),

$$L = L_*\left(\frac{\sigma}{\sigma_*}\right)^{\gamma}. \tag{4.3}$$

The measured relation is $L = L_*(\sigma_c/\sigma_{c*})^{\gamma}$ between luminosities and central velocity dispersions σ_c. The measured exponents are $\gamma = 3.7$ for E/S0 and $\gamma = 2.6$ for S galaxies with typical uncertainties of ± 1 (at 90% confidence) (de Vaucouleurs & Olson 1982). Following Fukugita & Turner (1991) we actually use $\gamma = 4$ for the E/S0 galaxies, and the results of § 5.4 show that the distinction is not important. The measured velocity dispersions of L_* E, SO, and S galaxies are $\sigma_{cE} = 225(+12; -20)$ km s^{-1}, $\sigma_{c0} = 206(+12; -20)$ km s^{-1}, and $\sigma_{cS} = 143(+8; -13)$ km s^{-1} in the B band (de Vaucouleurs & Olson 1982; Fukugita & Turner 1991).

4.2. *Isothermal Spheres and Galaxy Dynamics*

The statistical results are extremely sensitive to the estimated values of σ_*. Unlike the other input variables (n_*, α, quasar number counts) that depend only on counting accurately, the conversion between measured central velocity dispersions and the σ_* characterizing the mass distribution depends on theoretical interpretations of the observed central velocity dispersions σ_c. In addition to the 5%–10% statistical errors from fitting the observed distribution of central velocity dispersions, there can be systematic corrections for velocity anisotropies in the central regions (e.g., Tonry 1983), and differences in treating variations in the mass-to-light ratio. One standard systematic correction uses the argument from Gott (1977) that a $\propto r^{-3}$ tracer population of luminous matter in a $\propto r^{-2}$ isothermal dark matter halo has a velocity dispersion that is $(2/3)^{1/2}$ that of dark matter if the two populations are kinematically distinct. On the basis of this argument, Turner, Ostriker, & Gott (1984) advocated increasing the

velocity dispersion of the E and S0 galaxies by a factor of $(3/2)^{1/2}$ to convert the measured velocity dispersions of the luminous material into the velocity dispersion of the dominant dark matter distribution. Lens statistics are very sensitive to this correction because a 22% change in σ_* leads to a 50% change in image separations and a 125% change in the expected number of lenses. The general philosophy of this paper is to ignore classical dynamical measurements and to see how far we can go using the constraints from lensing alone. Nonethless, there are many dynamical measurements that bear on the value of the σ_* parameter, and we can ask what is the legitimate range of values for σ_* consistent with dynamical measurements.

Consider a spherical distribution of luminous matter $\nu(r)$ which is in a globally isothermal distribution with mass density $\rho(r) = \sigma_{DM}^2/(2\pi G r^2)$ and mass $M(r) = 2G\sigma_{DM}^2 r$. We measure the surface brightness profile $\Sigma(R)$ and the line-of-sight velocity dispersions $v_{los}(R)$ of the luminous matter, and we need to relate them to the value of σ_{DM} used in the lensing calculation. The luminous material has velocity dispersions σ_r^2, σ_θ^2, and σ_ϕ^2 with $\sigma_\theta^2 = \sigma_\phi^2 = (1-\beta)\sigma_r^2$ that must satisfy the Jeans equation

$$\partial_r(\nu\sigma_r^2) + 2\nu\beta\frac{\sigma_r^2}{r} = -2\nu\frac{\sigma_{DM}^2}{r}, \tag{4.4}$$

where the gravitational force is that of the isothermal halo rather than the self-gravity of the visible matter. The velocity dispersions satisfy a virial theorem found by taking the usual moment of the Jeans equation,

$$\langle\sigma_r^2 + \sigma_\theta^2 + \sigma_\phi^2\rangle_3 = G\frac{\int_0^\infty \nu M r\, dr}{\int_0^\infty \nu r^2\, dr} = 2\sigma_{DM}^2, \tag{4.5}$$

where the averages are the density-weighted volume averages of the dispersions $\langle\sigma^2\rangle_3 = \int d^3x\, \nu\sigma^2/\int d^3x\, \nu$. If we average the line-of-sight component of the velocity dispersion over the entire distribution using the Jeans equations, we find that

$$\langle v_{los}^2\rangle_2 = \frac{G}{3}\frac{\int_0^\infty \nu M r\, dr}{\int_0^\infty \nu r^2\, dr} = \frac{2}{3}\sigma_{DM}^2, \tag{4.6}$$

independent of the luminosity profile $\nu(r)$ and the anisotropy $\beta(r)$, where $\langle v_{los}^2\rangle_2 = \int d^2x\, \Sigma v_{los}^2/\int d^2x\Sigma$. The virial theorem and the global relationship between the line-of-site velocity and the halo are valid only if the luminous matter has finite mass and a core that is less singular than r^{-3}. Gott (1977) derived a correction factor by assuming $\nu(r) \propto r^{-3}$, in which case the relationship $\sigma_{DM}^2 = (3/2)v_{los}^2$ is true locally (for $\beta = 0$). Power-law profiles do not satisfy the global theorem because they have divergences either at the origin or at infinity when deriving the virial theorem. This proves that the correction $\sigma_{DM} = (3/2)\langle v_{los}^2\rangle_2^{1/2}$ is generic and independent of the distribution and isotropy of the luminous test particles.

In practice, no dynamical measurements ever determine this global average of the line-of-sight velocity. The average is always confined to some finite region around the center of the galaxy set by either the size of the aperture or the decreasing surface brightness of the galaxy. For a constant anisotropy β, the line-of-sight velocity dispersion at projected radius R is related to the dark matter dispersion and the luminosity profile by

$$v_{los}^2(R) = \frac{4\sigma_{DM}^2}{\Sigma(R)}\int_0^\infty du\left(1 - \frac{R^2}{u^2+R^2}\beta\right)\int_1^\infty dv\, v^{2\beta-1}\nu[(u^2+R^2)^{1/2}v], \tag{4.7}$$

where $\Sigma(R)$ is the surface density. Figure 1 shows v_{los}^2 and its surface brightness weighted average $\langle v_{los}^2\rangle_2(R)$ for the Hernquist (1990) and Jaffe (1983) models in which $\nu(r) \propto r^{-1}(r+a)^{-3}$ and $\propto r^{-2}(r+r_J)^{-2}$. The Hernquist (1990) model scale length is $a \simeq 0.45R_e$ and the Jaffe (1983) model scale length $r_J \simeq 1.31R_e$ where R_e is the de Vaucouleurs (1948) effective radius. Provided the orbits have $\beta \gtrsim -0.5$, the line-of-sight velocity dispersion declines with radius R. It is greater than the virial theorem value at small radii, crosses the virial theorem value near the scale radius $a(r_J)$, and is less than the virial theorem value outside. For isotropic orbits ($\beta = 0$) the limiting values are $2\sigma_{DM}^2$ for the Hernquist (1990) model and σ_{DM}^2 for the Jaffe (1983) model at the origin, and $\sigma_{DM}^2/2$ for both models at large radii. These limits are given by the asymptotic power-law forms of the potentials in the same manner as the original Gott (1977) derivation for an $\nu \propto r^{-3}$ power law.

If we take several galaxies from the sample examined by van der Marel (1991) and fit the velocity dispersions as function of radius with either a Hernquist (Jaffe) model or a Hernquist (Jaffe) profile as a tracer of an isothermal halo, we find that they give comparable statistical fits. The residuals do not seem to be much worse than the oblate models used by van der Marel (1991). The shape of the curves in Figure 1 show the results of the fitting procedure: the average velocity dispersion v_c within the central few arcseconds is roughly equal to the dark matter velocity dispersion. In the cases that overlap with de Vancouleurs & Olsen (1982) we find that the ratio of the dark matter dispersion to the central velocity dispersion is approximately $\sigma_{DM} \simeq 0.9$–$1.05v_c$ depending on the galaxy and the assumed isotropy of the orbits β. *This strongly suggests that the $(3/2)^{1/2}$ factor is not an appropriate correction to apply to lens statistics.*

This treatment neglects a number of systematic errors. We used a constant value for the anisotropy β, whereas it may well vary with radius. The measured line-of-sight velocities are all luminosity-weighted averages rather than mass-weighted averages. Any effects that lead to any variations of the luminosity per unit mass of the tracer population will lead to systematic errors. We expect these effects to be weak, but present, in E/S0 galaxies. We have not included a core radius in the isothermal potential both for the analytic simplicity and because we neglected the core radius in the lens calculations. The absence of central images in gravitational lenses and the other studies of lens statistics shows that the core radius must be smaller than a few 100 pc for L_* galaxies (Kochanek 1991a; Wallington & Narayan 1993; Krauss & White 1992). A slightly softened core on an L_* galaxy (<100 pc) has little effect on the lens statistics but it can change the relation between central velocity dispersions and σ_{DM}^2 by 5–10% by eliminating the central cusp in the dark matter. Such small cores have a much weaker effect on the relation between the average $\langle v_{los}^2\rangle$ and σ_{DM}^2.

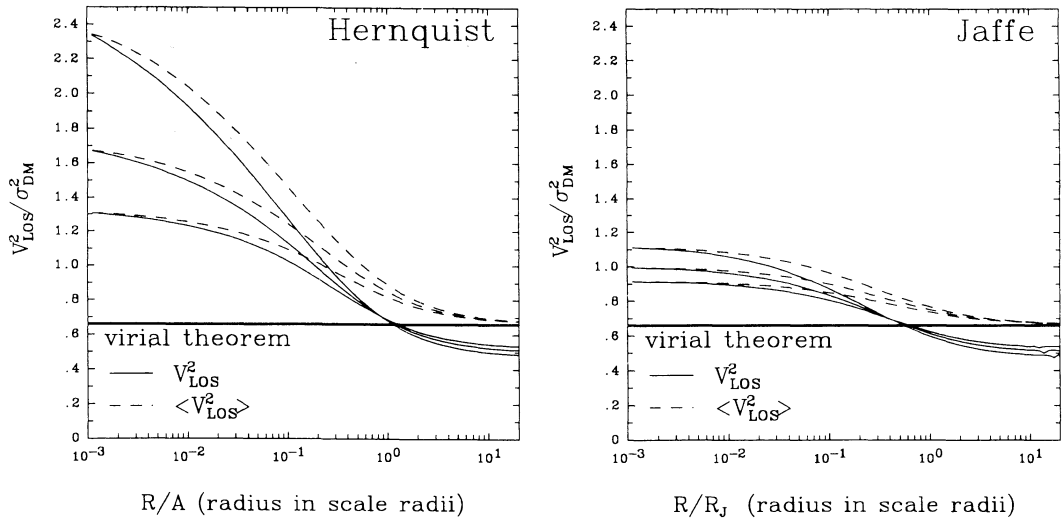

FIG. 1.—The relation between the line-of-sight velocity v_{los} and the dark matter velocity dispersion σ_{DM} for the Hernquist (1990) and Jaffe (1983) density models of ellipticals. The solid lines show the line-of-sight velocity dispersion at R, and the dashed lines show the surface density weighted average interior to R in units of σ_{DM}. The virial theorem requires that the average converge to (2/3) as shown by the heavy horizontal lines. The top curve in each triplet has slightly radial orbits ($\beta = 0.2$), the middle curve has isotropic orbits ($\beta = 0$), and the lower curve has slightly tangential orbits ($\beta = -0.2$).

Thus the dynamical uncertainties in σ_* are divided between a 7% statistical uncertainty from the measurements, and a 5–10% uncertainty from relating the isothermal velocity dispersion to the measured velocity dispersions. The average of the E/S0 velocity dispersions (weighted by lens optical depth) is $\sigma_* = 215$ km s^{-1}. If we divide the errors between a 7% statistical uncertainty for σ_{c*} measurements, a 5% statistical error for the conversion between σ_c and σ_*, and a 5% systematic error in the conversion, then the "90% confidence range" for σ_* is approximately 183 km s^{-1} to 248 km s^{-1}.

4.3. *Lensing by Singular Isothermal Spheres*

Under these assumptions, the optical depth for multiplying imaging a quasar is

$$\tau = \tau_* \Gamma[1 + \alpha + 4\gamma^{-1}] f(z) ,$$

where

$$\tau_* = 16\pi^3 n_* r_H^3 \left(\frac{\sigma_*}{c}\right)^4 , \tag{4.8}$$

the function

$$f(z) = \frac{1}{30} D_S^3 , \tag{4.9}$$

$r_H = c/H_0$ is the Hubble radius, and D_S is the proper motion distance to the source in a flat cosmology in units of r_H (Turner 1990). The cosmology is characterized by the ratio of the density of normal matter to the critical density, Ω_M, and the cosmological constant, Ω_Λ, where $\Omega_M + \Omega_\Lambda = 1$. We confine this study to flat cosmologies, because there is a large change in the optical depth between the Einstein-de Sitter model and cosmologies with a large cosmological constant.

A SIS lens with velocity dispersion σ has a critical radius of $b = 4\pi(\sigma/c)^2 D_{LS}/D_{OS}$ and image separation is $\Delta\theta = 2b$. The characteristic length scale $b_* = 1''.8(\sigma_*/250 \text{ km s}^{-1})^2$ is the critical radius produced by an L_* galaxy for a source at infinity ($D_{LS}/D_{OS} = 1$) (Gott & Gunn 1974) and the average critical radius in a flat cosmology is $\langle b \rangle = (b_*/2)\Gamma[1 + \alpha + 6\gamma^{-1}]/\Gamma[1 + \alpha + 4\gamma^{-1}]$. We use the critical radius rather than the image separation because the critical radius is a well-defined physical parameter in the models for the four image lenses such as PG 1115+080. The configuration probability that a lens in a flat universe has critical radius b is

$$p_c(b) = 30 \frac{\hat{b}^2}{b_*} \frac{\Gamma(1 + \alpha - 2\gamma^{-1}, \hat{b}^{\gamma/2}) - 2\hat{b}\Gamma(1 + \alpha - 4\gamma^{-1}, \hat{b}^{\gamma/2}) + \hat{b}^2\Gamma(1 + \alpha - 6\gamma^{-1}, \hat{b}^{\gamma/2})}{\Gamma(1 + \alpha + 4\gamma^{-1})} , \tag{4.10}$$

where $\hat{b} = b/b_*$ (Kaiser & Tribble 1992; Fukugita & Turner 1991; Kochanek 1993a). The fraction of lenses with critical radii larger than b is

$$g(>b) = \frac{\Gamma(1 + \alpha + 4\gamma^{-1}, \hat{b}^{\gamma/2}) - 10\hat{b}^3\Gamma(1 + \alpha - 2\gamma^{-1}, \hat{b}^{\gamma/2}) + 15\hat{b}^4\Gamma(1 + \alpha - 4\gamma^{-1}, \hat{b}^{\gamma/2}) - 6\hat{b}^5\Gamma(1 + \alpha - 6\gamma^{-1}, \hat{b}^{\gamma/2})}{\Gamma(1 + \alpha + 4\gamma^{-1})} , \tag{4.11}$$

which is a useful expression when calculating the selection function.

The final piece of the probability is magnification bias (Gott & Gunn 1974; Turner 1980), which corrects the optical depth for the magnification of the quasars from their original magnitude. The flux from the lensed images is magnified with an integral probability distribution of producing a magnification larger than M of $P(>M) = (M_0/M)^2$ for $M > M_0$, where $M_0 = 2$ is the minimum magnification of a multiply imaged source (Gott & Gunn 1974). We model the differential quasar number counts as a broken power law,

$$\frac{dN_q}{dm}(m) = \Sigma_0 \begin{cases} 10^{\alpha(m-m_0)}, & m < m_0, \\ 10^{\beta(m-m_0)}, & m > m_0, \end{cases} \tag{4.12}$$

where $\Sigma_0 = 10$ per square degree, $m_0 = 19.15$ B mag, $\alpha = 0.86$, and $\beta = 0.28$ (Hartwick & Schade 1990). The lens surveys and quasar catalogs usually use V magnitudes, so we use an average $B - V$ color of 0.2 as suggested by Maoz et al. (1993a, b).[2] We define the function

$$\mathscr{B}(m, M_1, M_2) = 2\left(\frac{dN_q}{dm}\right)^{-1} \int_{M_1}^{M_2} \frac{dM}{M^3} \frac{dN_q}{dm}(m + 2.5 \log M) =$$

$$= \begin{cases} \dfrac{2M_1^{-2+2.5\beta}}{2 - 2.5\beta}\left[1 - \left(\dfrac{M_1}{M_2}\right)^{2-2.5\beta}\right], & m > m_0, \\ \dfrac{2M_1^{-2+2.5\beta}}{2 - 2.5\beta}\left[1 - \left(\dfrac{M_1}{M_2}\right)^{2-2.5\beta}\right] 10^{(\beta-\alpha)(m-m_0)}, & m + 2.5 \log M_1 > m_0, \\ 2\left[\dfrac{1}{2.5\alpha - 2} + \dfrac{1}{2 - 2.5\beta}\right] 10^{(0.8-\alpha)(m-m_0)} - \dfrac{2M_1^{2.5\alpha-2}}{2.5\alpha - 2} - \dfrac{2M_2^{2.5\beta-2}}{2 - 2.5\beta} 10^{(\beta-\alpha)(m-m_0)}, & \begin{cases} m + 2.5 \log M_1 < m_0, \\ m + 2.5 \log M_2 > m_0, \end{cases} \\ \dfrac{2M_2^{-2+2.5\alpha}}{2.5\alpha - 2}\left[1 - \left(\dfrac{M_2}{M_1}\right)^{2-2.5\alpha}\right], & m + 2.5 \log M_2 < m_0, \end{cases} \tag{4.13}$$

to simplify the bias calculation. Usually we can allow the upper magnification cutoff M_2 to be infinite, although in practice we set it to be $M_2 = 10^4$ because we examine some values of β for which the magnification bias would diverge without a maximum magnification. If we are considering quasars, there is a real maximum in the magnification when the lensed source is faint enough to be a Seyfert rather than a quasar and we would expect to see the host galaxy as well as the active nucleus. The probability of multiply imaging a quasar with redshift z_i and B magnitude m_i in the absence of any selection effects is

$$p_i = \tau_* f(z_i) M_0^2 \mathscr{B}(m_i, M_0, \infty) \tag{4.14}$$

for the SIS model. (The bias factor defined by Fukugita & Turner 1991 is $B(m) = M_0^2 \mathscr{B}(m, M_0, \infty)$ with $M_0 = 2$.) In more complicated lens models or with the addition of selection effects, the factoring of the cross section and the magnification bias into independent, multiplicative terms cannot be done.

We can test for some systematic problems in using the SIS lens model by changing the value of M_0 in the magnification probability distribution. But when we change the average magnification, we must also change either the image separations or the cross section because the average magnification ($2M_0$) is proportional to the ratio of the square of the critical radius b to the cross section. If we think of changing M_0 as adding a constant density sheet to the lens model, then the scale of the critical radius must be changed to $b_* = 4\pi(\sigma_*/c)^2(M_0/2)^{1/2}$ when $M_0 \neq 2$ in a self-consistent model. The analogy to constant density sheets in the lens is correct, but using a constant value for M_0 means that the surface density of the sheet varies with redshift. Thus, this is an ad hoc model that allows us to test whether the survey statistics are consistent with the predictions of the pure SIS model in which $M_0 = 2$.

Observations have finite resolution and dynamic range, so we must include a selection function to correct the statistics for observational limitations. For the SIS model the selection effects can be characterized by the maximum magnitude difference that can be detected for two images separated by Δx, $\Delta m(\Delta x)$. If the flux ratio between the two images in an SIS lens is $f > 1$ ($2.5 \log f = \Delta m$), then the total magnification of the images is $M_f = M_0(f + 1)/(f - 1)$. Note that the larger the magnification, the closer the flux ratio is to unity. The survey can only detect lenses with magnifications larger than M_f, so that the magnification bias depends on the critical radius of the lens b because we must replace the M_0 in the standard bias function $[\mathscr{B}(m, M_0, M_2)]$ by the bias function with the limit on the detectable flux ratio $\mathscr{B}[m, M_f(b), M_2]$. The dependence of the selection function on the magnification means that the fraction of detectable lenses is not simply the fraction of all lenses with flux ratios smaller than Δm (which would be $[M_0/M_f]^2$), because the selection effects enter through changes in the magnification bias.

We decomposed the selection functions into the step functions given in Table 2 to allow rapid evaluation of the selection effects. The fraction of objects with critical radius b that can be detected is simply $\mathscr{B}[m, M_f(b), M_2]/\mathscr{B}(m, M_0, M_2)$, so the selection function corrected lens probabilities and separation probabilities are

$$p_i'(m) = p_i \int db\, p_c(b) \frac{\mathscr{B}(m, M_f(b), M_2)}{\mathscr{B}(m, M_0, M_2)}, \qquad p_{ci}'(b, m) = p_c(b) \frac{p_i}{p_i'} \frac{\mathscr{B}(m, M_f(b), M_2)}{\mathscr{B}(m, M_0, M_2)}. \tag{4.15}$$

[2] We also tried fitting the average $B-V$ color using the maximum likelihood method and the best-fit correction was statistically indistinguishable from the assumed value.

The effects of various selection functions on survey completeness as a function of image separation or velocity dispersion scale are discussed in Paper I. Near the expected values for σ_*, the surveys are 80%–90% complete.

In addition to the image separation, we can also use the configuration probabilities for the magnification and the lens redshift. The magnification of the two image lenses is easily defined from the flux ratio of the images, but we cannot fit the two four image lenses neatly into the statistics of the SIS lens. Statistical studies of elliptical lenses (Blandford & Kochanek 1987; Wallington & Narayan 1993) show that the shape of the total magnification probability distribution of elliptical SIS lenses is similar to that of circular SIS lenses. We use models of the four image lenses (Kochanek 1991a) and the SIS solution for the two image lenses to estimate the magnifications given in Table 1. The absolute magnification scale M_0 cannot be determined by models, so all the magnifications can be rescaled by changes in the value of M_0. Thus if we assume that the magnification probability distribution has the shape of the SIS distribution, the configuration probability for a lens with critical radius b, having magnification M, is

$$p'_M = \frac{2}{M^3}\frac{1}{\mathscr{B}(m, M_f(b), M_2)}\frac{(dN_q/dm)(m + 2.5 \log M)}{(dN_q/dm)(m)}, \tag{4.16}$$

where we have included the selection effects corrections. We know that we are making some systematic errors in estimating both the configuration probability and the magnifications, so we do not include this configuration probability in the standard likelihood analysis.

We know both the lens and source redshifts for four of the lenses in our sample, so we can use the configuration probability for a lens having both the observed separations and the observed redshifts in the analysis. The problem with using the redshift configuration probability is that it is difficult to define a redshift selection function to weight the probability to account for which redshifts are measurable. For example, we are more likely to measure the redshifts of large separation lenses because they tend to be brighter (Kochanek 1992a). If we ignore the selection effects, the configuration probability for finding a lens with critical radius b and redshift z_L in a flat cosmology is

$$p_{b,z} = \frac{15\gamma}{\Gamma(1 + \alpha + 4\gamma^{-1})}\frac{b}{b_*^2}\left(\frac{b}{b_*}\frac{D_S}{D_{LS}}\right)^{(1-\alpha)\gamma/2}\frac{D_L^2}{D_S^3}\frac{dD_L}{dz_L}\exp\left[-\left(\frac{b}{b_*}\frac{D_S}{D_{LS}}\right)^{\gamma/2}\right] \tag{4.17}$$

(Kochanek 1992a).[3] Since we do not fully understand the selection effects, we do not include the lens redshift configuration probability in our standard likelihood analysis.

5. MAXIMUM LIKELIHOOD MODELS OF LENS SURVEYS

The default parameters used in the study are a comoving density of $n_* = 5 \times 10^{-3} h^3$ Mpc^{-3} E/S0 galaxies in an Einstein-de Sitter cosmology ($\Omega_M = 1$, $\Omega_\Lambda = 0$) with Schechter function exponent $\alpha = -1$, "Tully-Fisher" exponent $\gamma = 4$, and $B-V = 0.2$ color for quasars. The velocity dispersion scale σ_* is always regarded as a variable to be determined by the lens statistics, and the minimum magnification is $M_0 = 2$. The quasar luminosity function is fixed to the simple model with a bright end slope $\alpha = 0.86$, a break at $m_0 = 19.15$ B mag, and a faint end slope of $\beta = 0.28$. Spiral galaxies, when they are included, have comoving density $n_* = 1.5 \times 10^{-2} h^3$ Mpc^{-3} and velocity dispersion scale $\sigma_* = 150$ km s^{-1}. The likelihood function uses the lensed and unlensed likelihoods for the quasars in the Snapshot Survey, Crampton et al. (1992), and Yee et al. (1992) surveys, and the image separation configuration probability for the five optical lenses and the eight radio lenses listed in Table 1. All likelihoods are weighted by the selection functions given in Table 2. The major source of systematic error is the treatment of the lens 0957+561, and we derive our results both with and without this lens to show the magnitude of the uncertainties.

The first, and most important, test of our statistical model is whether the statistical model is consistent with the data at all. We used the maximum likelihood model for the default parameters in an Einstein-de Sitter universe and the best-fit velocity dispersion excluding 0957+561 to generate Monte Carlo simulations of observations of the Snapshot Survey. The value of the likelihood for the real survey is near the median of the likelihoods from the Monte Carlo simulations. For example, if we fit only the Snapshot Survey data, 55% of Monte Carlo simulations had lower likelihoods than that found with 0957+561 excluded, and 28% had lower likelihoods than that found with 0957+561 included. The total ensemble of Monte Carlo simulations includes the Poisson fluctuations in the number of lenses. If we restrict ourselves to realizations that found four lenses, then 90% of the Monte Carlo simulations had likelihoods lower than that found with 0957+561 excluded, and if we restrict ourselves to realizations that found five lenses, 44% had likelihoods lower than that found with 0957+561 included. In short, the measured peak likelihoods are typical of Monte Carlo realizations drawn from the SIS model, so there is no statistical reason to reject the SIS model.

The maximum of the likelihood $L_{\max}$ as a function of the parameters is the best estimator for the parameters of the model, and the logarithm of the likelihood ratio $-2\ln(L/L_{\max})$ is asymptotically distributed like the χ^2 distribution (e.g., Lupton 1993). In all the figures we present likelihood contours as a function of two parameters, so the 68% (1 σ), 90%, 95.4% (2 σ) and 99% confidence levels on the parameters in two dimensions are the contours on which the likelihoods are fraction 32%, 10%, 4.5%, and 1% of the maximum. The confidence interval on one parameter is determined by the extrema of the parameters on the contours with the likelihoods for the χ^2 distribution with one degree of freedom, so the 68% (1 σ), 90%, 95.4% (2 σ) and 99% confidence limits on a single parameter in the two-dimensional spaces are the extreme values of the parameter on the contours at 61%, 26%, 14%, and 3.6% of the peak likelihood. Sometimes we examined variations of three parameters simultaneously, but we never quote errors for these cases. In the three parameter spaces we examined there is always a near degeneracy that prevents a simultaneous estimate of

[3] The expression in Kochanek (1992a) is the probability distribution in b/b_* rather than b, which is the origin of the extra b_*^{-1} here.

all three variables. Figure 2 shows how the three components of the likelihood function depend on the velocity dispersion scale. In § 5.1 we examine trade offs between velocity dispersions and cosmological models, in § 5.2 we examine the role of spiral galaxies, and in § 5.3 we examine the number density of E/S0 galaxies. In § 5.4 we check to see if the assumptions of a Schechter distribution and a "Tully-Fisher" relation are valid. In § 5.5 we check the quasar number count distribution, and in § 5.6 we check the minimum magnification of the lens model.

5.1. *Galaxy Velocity Dispersions and Cosmological Model*

The expected number of lenses in a given cosmological model scales as $\sigma_*^4\langle f\rangle$ where $\langle f\rangle$ is the average of the optical depth function (4.9). The traditional approach to this problem is to use a fixed value of σ_* based on observations of central velocity dispersions plus a dynamical model, compute the expected number of lenses as a function of the cosmological model, and finally apply Poisson statistics to limit the cosmological model (e.g., Turner 1990; Fukugita & Turner 1991; Snapshot Survey). The weakness of this approach is that including the $(3/2)^{1/2}$ correction factor in the velocity dispersions strongly biases the results against allowing a large cosmological constant. Thus the derived limits on the cosmological model depended entirely on the assumed value of σ_*.

The lensed systems, however, provide us with completely independent information on the mass scale because the image separations depend on σ_*^2 and are almost independent of cosmology (Kochanek 1993a). If we include the configuration parameter for the image separations, we can simultaneously estimate σ_* and the cosmological model. The number of lenses in the sample limits how well the mean image separation is determined, but the dominant uncertainty is how to treat 0957+561, which has an anomalously large separation because the lens is a combination of a galaxy and a cluster. We always compute our results both with and without 0957+561 included as a lensed quasar to show the level at which the ambiguity modifies our results.

The maximum likelihood with 0957+561 included has $\Omega_M = 1.04$ and $\sigma_* = 275$ km s^{-1}, while the maximum without 0957 + 561 has $\Omega_M = 0.72$ and $\sigma_* = 240$ km s^{-1}. If we restrict ourselves to the Einstein-de Sitter cosmology ($\Omega_M = 1$), then the estimates for the velocity dispersions are $\sigma_* = 275$ km s^{-1} and $\sigma_* = 245$ km s^{-1} and the reductions in the likelihood from the peak are negligible in both cases. Contour plots of the likelihoods as a function of Ω_M and σ_* are shown in Figure 3. Because the surveys are 80%–90% complete for these velocity dispersions, the likelihood peaks are only slightly modified by the addition of the selection effects. The lower likelihood contours do change appreciably with the addition of selection effects. In particular the outer limit of the search area in the Snapshot Survey at 7.″0 reduces the restrictions on large values of σ_*. Figure 2 shows how much broader the 90% confidence limits on σ_* become if we use only the Snapshot Survey data. The estimate of σ_* without 0957+561 is consistent with the dynamical estimates from § 4.2, although the error estimates are broader. With 0957+561 it is not consistent, which is expected because a cluster contributes to the image separation.

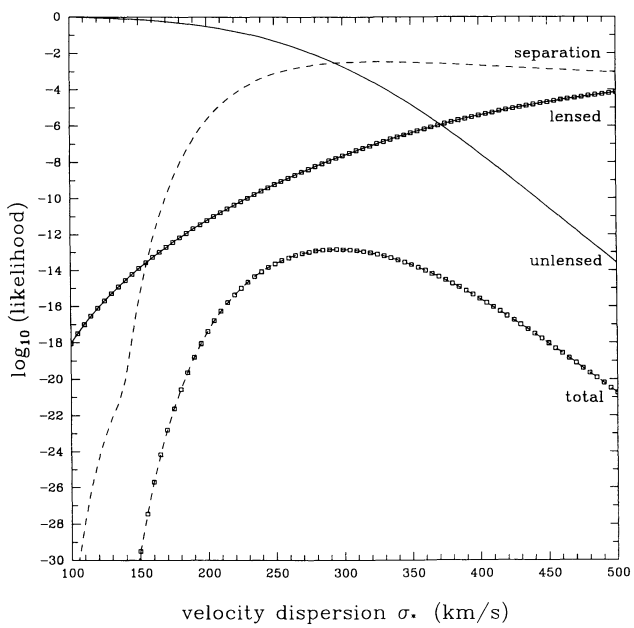

FIG. 2

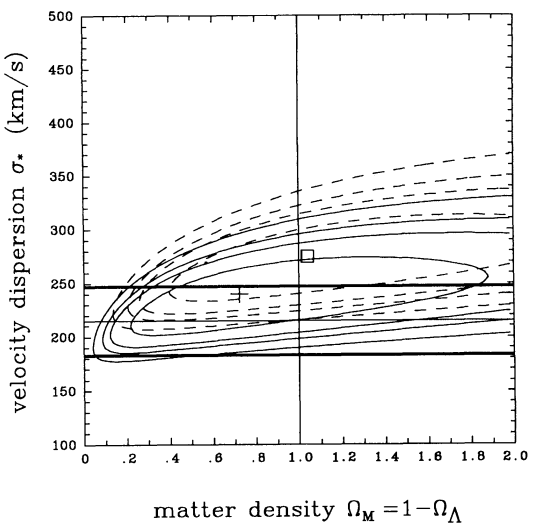

FIG. 3

FIG. 2.—Variation of the likelihood terms with the velocity dispersion scale σ_* in the Einstein-de Sitter universe. The likelihoods are computed using only the Snapshot Survey data and include 0957+561. The solid line shows the likelihood that the unlensed quasars are unlensed, and the solid line with points shows the likelihood that the lensed quasars are lensed. The dashed line shows the likelihood for the observed image separations for the five lenses, and the dashed line with points is the total likelihood.

FIG. 3.—Likelihood contours for flat cosmologies in the space of the velocity dispersion scale σ_* and the matter density $\Omega_M = 1 - \Omega_\Lambda$. The solid lines show the likelihood contours excluding 0957+561, and the dashed lines show the likelihood contours including 0957+561. The peak likelihood with 0957+561 is marked by the square, and the peak without 0957+561 is marked by the cross. Contours lie at the 68% (1 σ), 90%, 95% (2 σ), and 99% confidence levels of the likelihood ratio for two parameters. The vertical line marks the default Einstein-de Sitter cosmology. The light horizontal line is the dynamical estimate of σ_*, and the heavy horizontal lines mark the dynamically estimated range for σ_*.

The steep rise in the optical depth as $\Omega_\Lambda \to 1$ does allow us to set an upper limit on the cosmological constant, although the absence of prior assumptions about the value of σ_* weakens the limits, particularly if we exclude 0957+561. The presence of 0957+561 forces a large value for σ_* (so that there is an appreciable probability of producing its large separation), leading to a strong limit on the cosmological constant. The 90% confidence limit on Ω_Λ is $\Omega_\Lambda \lesssim 0.65$ when 0957+561 is included, and $\Omega_\Lambda \lesssim 0.8$ when it is excluded. The cause of the weak limit on Ω_Λ without 0957+561 is the low E/S0 velocity dispersion of about $\sigma_* \simeq 200$ km s^{-1} at the maximum value of Ω_Λ. This dispersion is consistent with the dynamical estimates for σ_* in § 4.2, and it shows that gravitational lensing can only rule out large values for the cosmological constant at high levels of confidence. If we did not include the configuration probabilities for the radio-selected lenses, these limits become even weaker.

If we restrict ourselves to an Einstein-de Sitter universe, the uncertainties in the range for the value of σ_* are similar to those from dynamical studies. Excluding 0957+561 we can limit its range to 210 km s^{-1} $\lesssim \sigma_* \lesssim$ 270 km s^{-1} at 90% confidence, while the presence of 0957+561 pushes the range upward to 240 km s^{-1} $\lesssim \sigma_* \lesssim$ 300 km s^{-1}. The lower limits match the measured values of 200–220 km s^{-1}, while the upper limits are comparable to the 270 km s^{-1} advocated by Turner (1990). Since we know that 0957+561 is an aberration that biases the velocity dispersions upward, we conclude that any correction to the observed velocity dispersions to account for the effects of dark matter halos is smaller than the $(3/2)^{1/2}$ suggested by Gott (1977), and the models without 0957+561 agree with the dynamical estimates.

5.2. *The Role of Spiral Galaxies*

Spiral galaxies are 3 times more numerous than E/S0s but the low-velocity dispersion scale of spirals ($\sigma_{*S} \simeq 150$ km s^{-1}) and the strong scaling of cross section with velocity dispersion ($\propto \sigma_*^4$) means that the E/S0 galaxies dominate the lensing cross section provided $\sigma_{*E} \gtrsim 190$ km s^{-1}. This is slightly smaller than the measured values for E/S0 galaxies. Since the maximum likelihood in the elliptical-only models is above 200 km s^{-1}, the presence of spirals will only weakly modify the location of the peak in the likelihood function.

The lensing phenomenon is dominated by the mass in the inner few kiloparsecs of the lens galaxy, where there is abundant information on the mass of spiral galaxies from rotation curves. This probably means that the mass estimates for lensing by spirals are more robust than for early-type galaxies, and we will not examine the effects of variations in the velocity dispersion scale. We should keep in mind, however, that other effects such as finite core radii can suppress the lensing cross sections of spiral galaxies (Krauss & White 1992; Kochanek 1991b; Wallington & Narayan 1993), but this will simply make the likelihood distributions relax back toward the results with no spirals.

If we add spirals with number density $n_* = 1.5 \times 10^{-2} h^3$ Mpc^{-3} and velocity dispersion $\sigma_* = 150$ km s^{-1} there is a negligible effect in the maximum of the likelihood or the estimated velocity dispersion for the E/S0s. The peaks shift toward larger matter densities, Ω_M, because of the flat ridge in the likelihood. With 0957+561 the peak is at $\Omega_M = 1.32$ and $\sigma_* = 280$ km s^{-1}, and without 0957+561 the peak is at $\Omega_M = 1.06$ and $\sigma_* = 245$ km s^{-1}. In an Einstein-de Sitter universe the preferred velocity dispersions are $\sigma_* = 270$ km s^{-1} with 0957+561, and $\sigma_* = 245$ km s^{-1} without it. The likelihoods are shown in Figure 4. The addition of the spirals does not markedly increase or decrease the likelihoods relative to the model with no contribution from spirals at all: the fits are slightly worse in both cases with a reduction in the peak likelihood by a factor of 1.3 without 0957+561, and 1.5 with 0957+561. The presence of the spirals strengthens the case against a cosmological constant because the contribution of the spirals to the optical depth becomes important just when the E/S0 velocity dispersion becomes small enough to allow a large cosmological constant. The 90% confidence limits on Ω_Λ are $\lesssim$0.45 with 0957+561, and $\lesssim$0.6 without 0957+561.

5.3. *Galaxy Number Density*

The observed galaxy number counts cannot exclude the possibility of a population of dark galaxies. Such halos have been suggested as the lenses in several of the large separation quasar pairs (see Surdej et al. 1992 for a review of these objects). We test for dark halos by optimizing the density of E/S0 galaxies n_*. We must do this in a fixed cosmology, because the expected number of lenses depends on $n_* \langle f \rangle$ and has no effect on the image separations. Thus the likelihood must disentangle the effects of the galaxy number density and the cosmological model using the leverage from the variations in optical depth with redshift, which are too weak to constrain the model with the current data. The degeneracy can be broken by either a sample with many more lenses, or by determining the lens redshifts in the existing sample. Varying n_* also tests for problems in the lens model, because we can regard a change in n_* as a change in the lens cross section to $(n_*/n_{*0})\sigma_*^4$ rather than a change in the density of galaxies. This mimics some of the effects of adding a core radius to the lens model.

The variation of the likelihood with n_* is shown in Figure 5. The fitted value of n_* in this E/S0 only model is $n_* = 0.0048h^3$ Mpc^{-3} with 0957+561, and $n_* = 0.0067h^3$ Mpc^{-3} without 0957+561, with 90% confidence ranges of $0.0017 \lesssim n_* h^3$ Mpc^{-3} $\lesssim$ 0.011 with 0957+561 and $0.0020 \lesssim n_* h^3$ Mpc^{-3} $\lesssim 0.017$ without 0957+561, compared to an observed value from galaxy number counts of $0.005 \pm 0.0026h^3$ Mpc^{-3} where the error is modified to be a 90% confidence interval. Lensing statistics support neither the existence of dark halos compact enough to cause gravitational lensing, nor large deviations of the cross section from the SIS predictions, although the range of the uncertainties is still large compared to the measured densities.

5.4. *Schechter Function Slope and "Tully-Fisher" Exponent*

As a related test we can discard all the observational information on galaxy number counts and velocity dispersions and try to determine the distribution of isothermal halos based only on gravitational lensing. As a practical, computational matter we can study different distributions in the three-dimensional spaces of σ_*, n_* and one of α and γ with the other fixed. The maximum likelihood technique tries to match both the expected number of lenses ($\propto n_* \sigma_*^4 \Gamma[1 + \alpha + 4\gamma^{-1}]$) to the observed number, and the mean image separation ($\propto \sigma_*^2 \Gamma[1 + \alpha + 6\gamma^{-1}]/\Gamma[1 + \alpha + 4\gamma^{-1}]$) to the observed mean. If we fix the expected number of lenses and

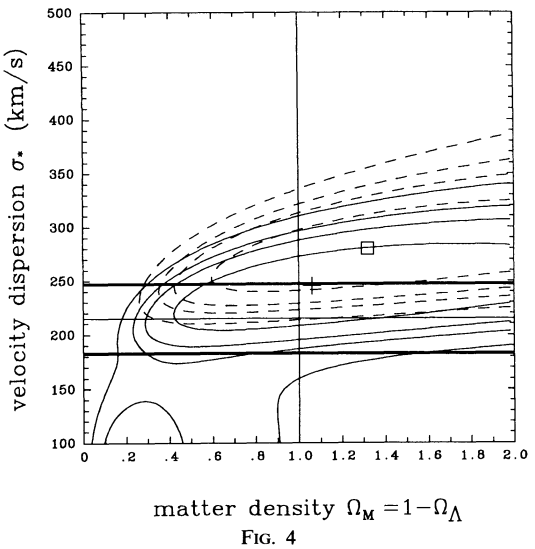

FIG. 4

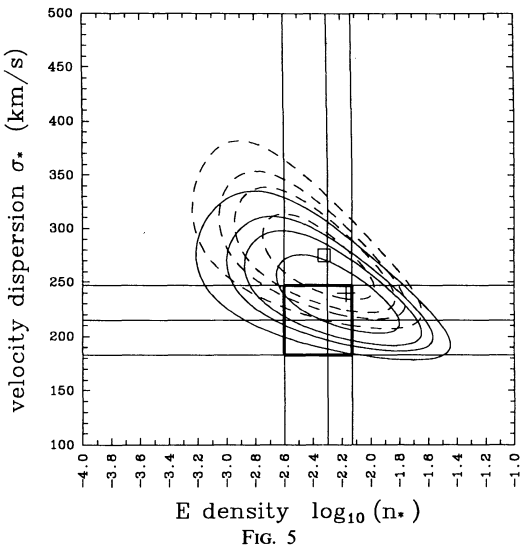

FIG. 5

FIG. 4.—Likelihood contours for flat cosmologies in the space of the velocity dispersion scale σ_* and the matter density $\Omega_M = 1 - \Omega_\Lambda$ with the addition of spiral galaxies. The solid lines show the likelihood contours excluding 0957+561, and the dashed lines show the likelihood contours including 0957+561. The peak likelihood with 0957+561 is marked by the square, and the peak without 0957+561 is marked by the cross. Contour spacing is the same as in Fig. 3. The vertical lines marks the default Einstein-de Sitter cosmology.

FIG. 5.—Likelihood contours in the space of velocity dispersion scale σ_* and the number density of ellipticals n_* (in units of h^3 Mpc^{-3}) in an Einstein-de Sitter cosmology. The vertical line marks the observed density of E/S0 galaxies, with a 90% confidence error bar on the measured value. The heavy solid box is the allowed range estimated from galaxy number counts and dynamics. Contour spacing is the same as in Fig. 3.

the density of L_* galaxies, then the mean separation of the images varies as $\Gamma[1 + \alpha + 6\gamma^{-1}]\Gamma[1 + \alpha + 4\gamma^{-1}]^{-3/2}$ when we change α and γ. When we vary α the mean separation has a peak near $\alpha = 0$ and then decreases for both larger and smaller values, and when we increase γ the mean separation decreases monotonically. Thus there will typically be two solution regions as we vary α, one on either side of the maximum, and one solution region for γ. The addition of the selection effects tends to broaden the allowed range of solutions, although the outer survey boundary chosen by the observers has a stronger effect than the inner boundary from instrumental resolution.

The likelihood contours as we vary α or γ with a fixed galaxy density n_* are shown in Figures 6 and 7. In both cases the value of the parameter is weakly determined, although values of α smaller than $\alpha \lesssim -1.6$ are ruled out. If we include 0957+561, then the value

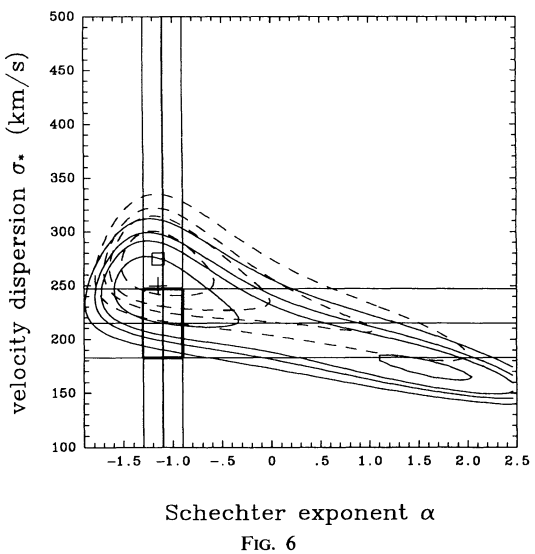

FIG. 6

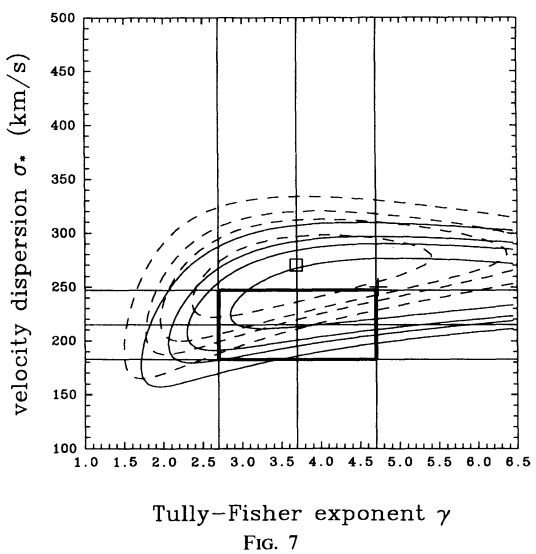

FIG. 7

FIG. 6.—Likelihood contours in the space of Schechter exponent α and velocity dispersion scale σ_* for a fixed galaxy number density n_* equal to the density of E/S0 galaxies. The vertical line marks the observational value for $\alpha \simeq -1.1$, with a 90% confidence error bar on the measured value. The heavy solid box is the allowed range estimated from galaxy number counts and dynamics. Contour spacing is the same as in Fig. 3. There is a secondary minimum in the results without 0957+561 (*solid lines*) near $\alpha = 1.5$.

FIG. 7.—Likelihood contours in the space of Tully-Fisher exponent γ and velocity dispersion scale σ_* for a fixed galaxy number density n_* equal to the density of E/S0 galaxies. The vertical line marks the assumed value of $\gamma \simeq 4$ and a 90% confidence error level in the estimated value. The heavy solid box is the allowed range estimated from galaxy number counts and dynamics. Contour spacing is the same as in Fig. 3.

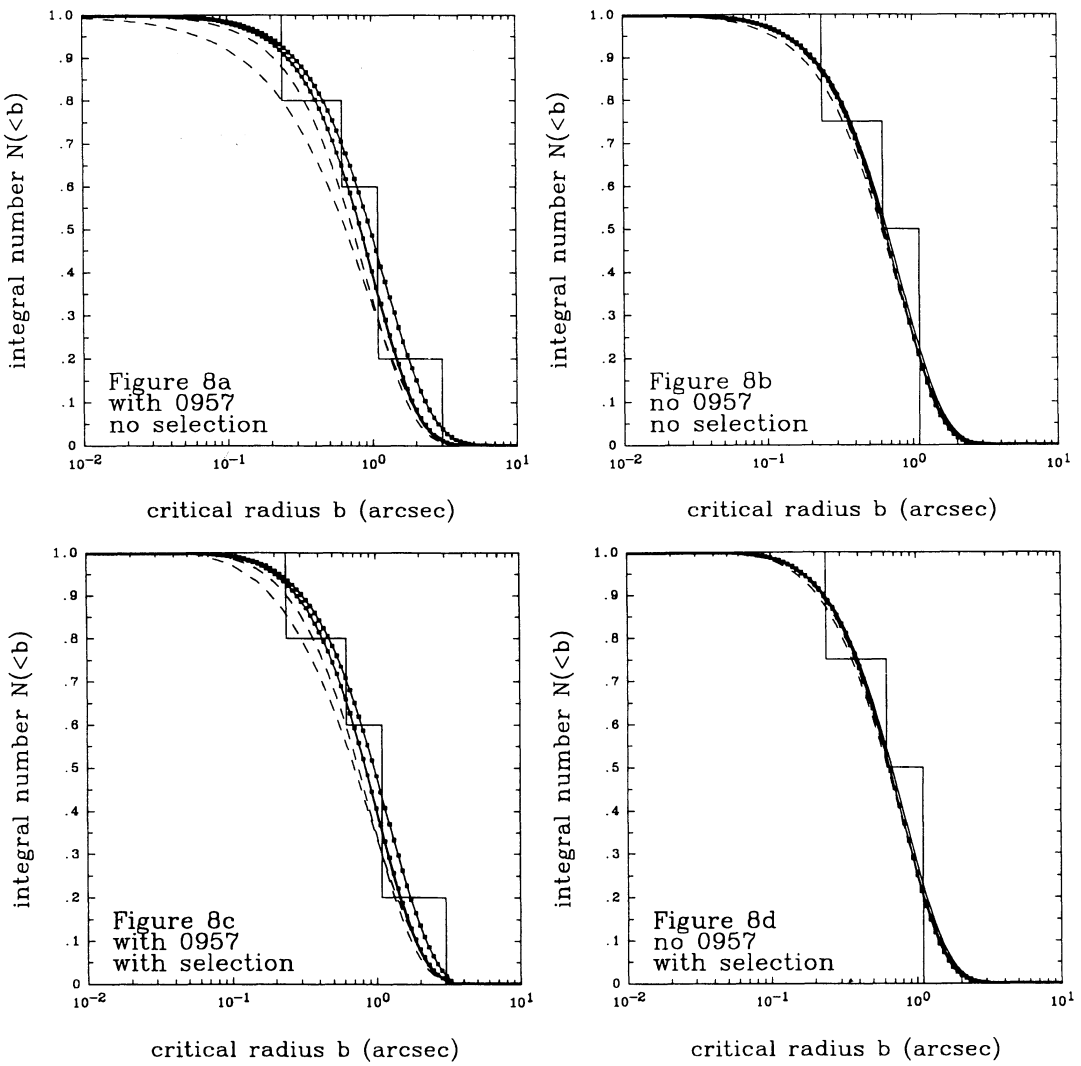

FIG. 8.—Integral distributions of critical radii b. Figs. 8*a* and 8*b* show the true distributions before applying the Snapshot Survey selection function, and 8*c* and 8*d* show the distributions after applying the selection function. The solid histograms show the observed distribution of lenses. There are six different fits in each figures. The solid lines have $\alpha = -1$, $\gamma = 4$ and either the observed value for n_* or the best-fit value from the lens model. The two dashed lines show the effects of varying α with n_* either fixed or optimized, and the solid lines with points show the effects of varying γ with n_* either fixed or optimized. No distribution is significantly better than the rest. The selection function assumes the lenses are 17th mag.

of α is bounded between $-1.5 \lesssim \alpha \lesssim -0.5$ and the likelihood peak lies near the observed value. Without 0957+561, there is a long crest of nearly equal likelihoods. Small values of γ have a weaker cutoff for large image separations, so the inclusion of 0957+561 biases the solutions to smaller values of the "Tully-Fisher" exponent.

The parameters α and γ are weakly constrained because there are too few lenses to determine the shape of the distribution in image separation. The best-fitting models are all similar, and their integral distributions ae shown in Figure 8. We show both the true distribution and the distribution after applying the Snapshot Survey selection function (assuming a 17th magnitude lens). The best model with 0957+561 has $\alpha = -1.46$, $\gamma = 4$, $\sigma_* = 315$ km s^{-1}, and $n_* = 0.0018$ and its likelihood is 1.5 times that of the default model. The best model without 0957+561 has $\alpha = -1$, $\gamma = 4$, $\sigma_* = 240$, and $n_* = 0.0067$ and its likelihood is 1.1 times that of the default model. In short, there are too many degeneracies between the four variables (α, γ, σ_*, and n_*) to measure them all with the current data, but no variations in the three variable subspaces we examine significantly improve on the default values.

5.5. *Quasar Luminosity Function*

The amount of magnification bias depends on the shape of the quasar luminosity function and on the magnification probability distribution of the lenses. The quasar apparent magnitude number counts (4.8) depend on the bright slope $\alpha = 0.86$, the faint slope $\beta = 0.28$, and a break magnitude $m_0 = 19.15$ B mag where increasing the slopes or decreasing the break magnitude increases the expected number of lenses. The likelihood contours for variations in α, β, and m_0 are shown in Figures 9, 10, and 11.

Most of the magnification bias is determined by the bright end slope α and the position of the break in the number counts m_0. Because almost all of the survey quasars are brighter than m_0, the results are less sensitive to the faint end slope β. For a fixed break

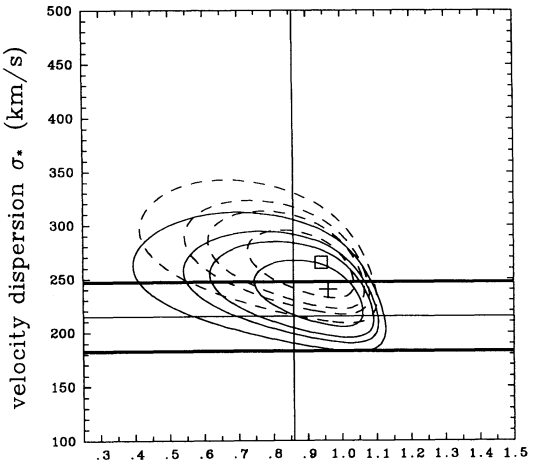

FIG. 9

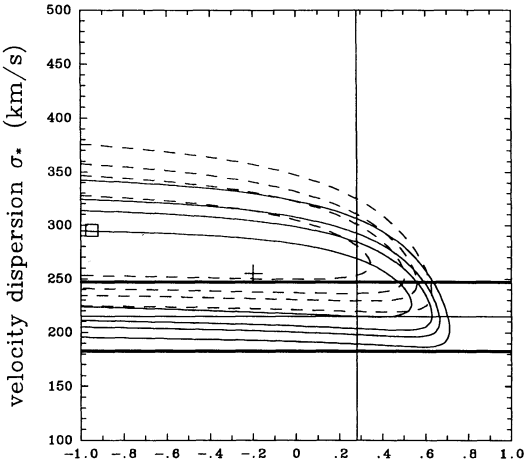

FIG. 10

FIG. 9.—Likelihood contours in the space of the slope of the bright end of the quasar luminosity function and the velocity dispersion scale σ_*. The vertical line marks the observational value of $\alpha \simeq 0.86$. Contour spacing is the same as in Fig. 3.

FIG. 10.—Likelihood contours in the space of the slope of the faint end of the quasar luminosity function and the velocity dispersion scale σ_*. The vertical line marks the observational value of $\beta \simeq 0.28$. Contour spacing is the same as in Fig. 3.

magnitude of $m_0 = 19.15$, the fits give steeper bright slopes: $\alpha = 0.94$, $\sigma_* = 265$ km s^{-1} with 0957+561, and $\alpha = 0.96$, $\sigma_* = 240$ km s^{-1} without 0957+561. The standard model is well within the 90% confidence limit and the increase in the likelihood is a factor of 1.3 in both cases. The preferred solutions have negative faint end slopes. In the case with 0957+561 the likelihoods increase by a factor of 2.3 at $\beta = -1$ relative to $\beta = 0.28$, although the changes are much less dramatic without 0957+561 ($\beta = -0.2$, likelihood increases by a factor of 1.2). The improvements come from reducing the likelihoods that the unlensed quasars are lensed. The models prefer a brighter break magnitude near $m_0 = 18.75$ with 0957+561, $m_0 = 19.05$ without 0957+561. The likelihood with 0957+561 improves by a factor of 1.3 with the change in the break magnitude. All these changes are in the direction of increasing the magnification bias for bright quasars while reducing the bias for fainter quasars. The reason for the change in this direction is that the lenses all hug the brightest end of the distribution of observed quasars, whereas lenses produced using SIS statistics and the standard parameters for the magnification bias tend to be more uniformly distributed.

We can strengthen the constraints on the terms that change the magnification bias by adding the magnification configuration probability (eqn. [4.6]) for the optical lenses. The magnification configuration probability depends only on the properties of the quasar luminosity function and M_0, so it helps to break the degeneracy between these quantities and the velocity dispersion. Figures 12, 13, and 14 show the likelihoods for the quasar number count parameters when we include the magnification configuration

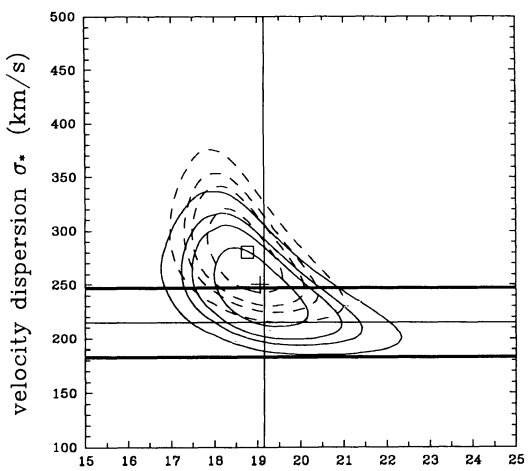

FIG. 11

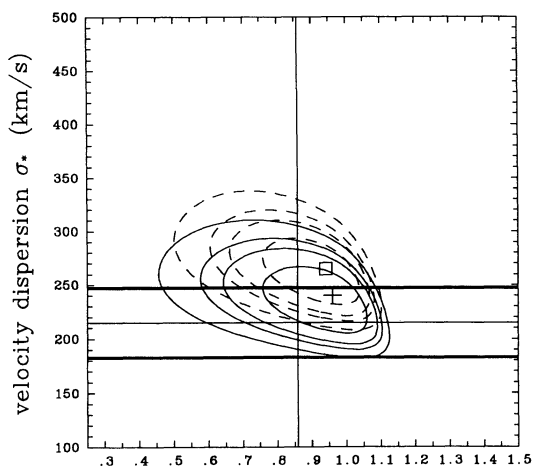

FIG. 12

FIG. 11.—Likelihood contours in the space of break magnitude of the quasar luminosity function and the velocity dispersion scale σ_*. The vertical line marks the observational value of $m_0 \simeq 19.15$. Contour spacing is the same as in Fig. 3.

FIG. 12.—Likelihood contours in the space of the slope of the bright end of the quasar luminosity function and the velocity dispersion scale σ_* with the addition of the magnification configuration probability. The vertical line marks the observational value of $\alpha \simeq 0.86$, and the contour spacing is the same as in Fig. 3.

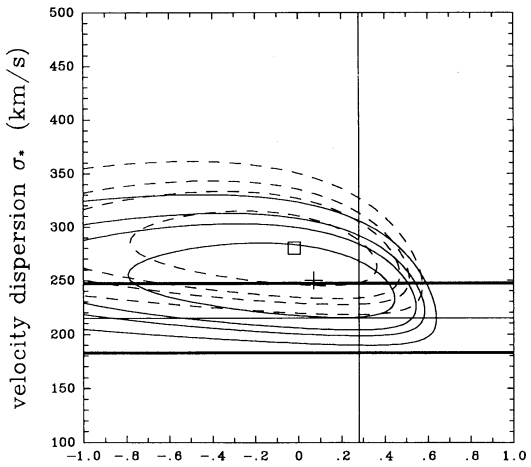

FIG. 13

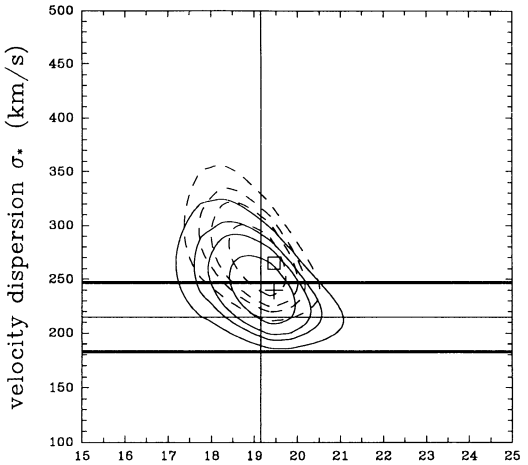

FIG. 14

FIG. 13.—Likelihood contours in the space of the slope of the faint end of the quasar luminosity function and the velocity dispersion scale σ_* with the addition of the magnification configuration probability. The vertical line marks the observational value of $\beta \simeq 0.28$, and the contour spacing is the same as in Fig. 3.

FIG. 14.—Likelihood contours in the space of break magnitude of the quasar luminosity function and the velocity dispersion scale σ_* with the addition of the magnification configuration probability. The vertical line marks the observational value of $m_0 \simeq 0.86$, and the contour spacing is the same as in Fig. 3.

probability. In each case the peaks of the likelihood are shifted in the direction of agreeing with the observational values. This is particularly evident for the faint end slope β, where the peak shifts to $\beta = -0.02$ with 0957+561 and to 0.06 without 0957+561, greatly reducing the discrepancies seen in Figure 10. The bright end slope estimate remains somewhat steeper than the observed value and the peak for the break magnitude rises to 19.45.

5.6. *Minimum Magnification*

The final possibility we examine is whether the SIS model correctly estimates the typical magnification produced by gravitational lenses. We know the magnification probability distribution is dominated by folds, which gives the characteristic slope to the distribution, but we have no direct evidence for the value of the minimum magnification M_0. Figure 15 shows the likelihood contours for variations in σ_* and M_0. The peaks have substantially higher minimum magnifications, $M_0 = 5.8$ with 0957+551, and $M_0 = 3.6$ without 0957+561, and the likelihood for the 0957+561 model peak is 7.4 times that for the point with $M_0 = 2$. When we add the configuration probability for the image flux ratios, most of the differences vanish (see Fig. 16). The results favor a smaller mean magnification than the SIS model, but the differences between the peak and the SIS model are greatly reduced.

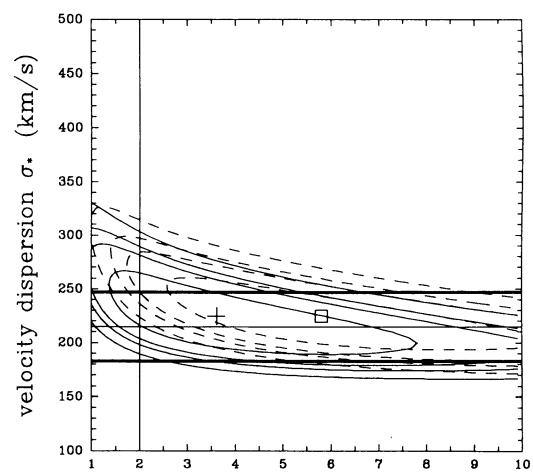

FIG. 15

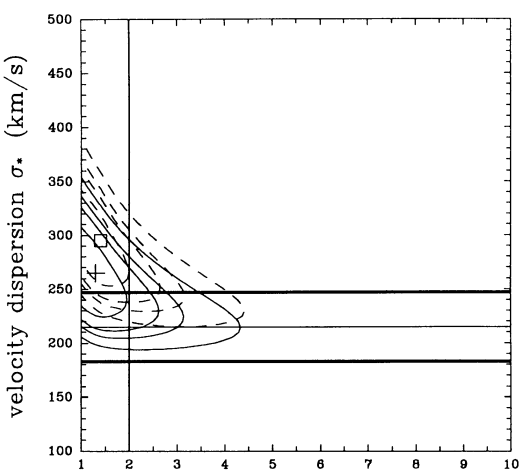

FIG. 16

FIG. 15.—Likelihood contours in the space of minimum magnification and velocity dispersion scale. The SIS value of $M_0 = 2$ is marked by the vertical line. The contour spacing is the same as in Fig. 3.

FIG. 16.—Likelihood contours in the space of minimum magnification and velocity dispersion scale with the addition of the magnification configuration probability. The SIS value of $M_0 = 2$ is marked by the vertical line. The contour spacing is the same as in Fig. 3.

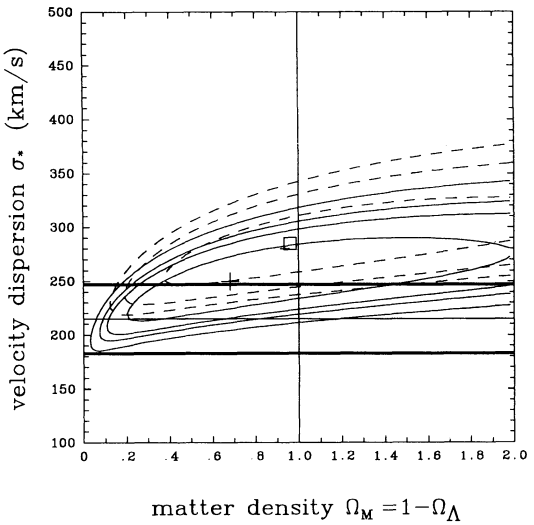

FIG 17. Likelihood contours in the space of matter density and velocity dispersion scale where we have used the lens redshift configuration probability instead of just the separation configuration probability for the four lenses in which both redshifts are known. This should be compared to the results in Fig. 3. The Einstein–De Sitter cosmology is marked by the vertical line, and the contour spacing is the same as in Fig. 3.

6. WHAT CAN BE DONE TO IMPROVE THE STATISTICS

The parameters derived from the Snapshot Survey with the addition of the lenses from the large radio surveys cannot as yet distinguish between most cosmologies or constrain any observational input to the calculation more tightly than other observational techniques. We are, however, close to this point, and we can ask what observations would increase the constraints most rapidly.

6.1. *Including More Surveys or Known Lenses*

The addition of the remaining large optical survey (the ESO/Liège Survey) will not substantially improve the constraints because of the huge overlap between the four surveys. The large radio surveys can improve the constraints on cosmological models provided the selection effects of the surveys can be understood, and we know the source redshift and flux distributions. The most important problem for limiting the cosmological model is understanding the selection effects, because cosmological limits depend on accurately estimating the completeness of the survey.[4] The addition of more lenses will continue to strengthen the limits on the mass scale of galaxies. There are three more lenses found independently from the large surveys, which could be included if their selection effects were understood.

6.2. *Lens Redshifts*

If we see a lens with critical radius b then a model with critical radius scale b_* has a cutoff in the likelihood for small velocity dispersions (small b_*) that is proportional to $\exp(-(b/b_*)^{\gamma/2})$ when $b > b_*$. This causes an exponential cutoff in the likelihood when an L_* galaxy at zero redshift cannot produce the observed separation. If we know the lens redshift as well as the image separation, the exponential cutoff changes to $\exp\{-[(b/b_*)(D_S/D_{LS})]^{\gamma/2}\}$ and the likelihood declines exponentially when an L_* galaxy at the observed redshift cannot produce the observed separation. Since the average lens has $D_S/D_{LS} = 2$ (Kochanek 1993a), the major effect of adding the information from lens redshifts is to sharpen the cutoff in the likelihoods for small velocity dispersion scales. Unfortunately there are few systems for which we know the lens redshifts, particularly among the systems found by examining bright quasars—choosing bright quasars automatically makes it difficult to measure lens redshifts. We have four lenses in which we know both the source and the lens redshift (0957+561, 0142−100, 2016+112, and 1654+134).

The results using the lens redshift configuration probability instead of the separation configuration probability are shown in Figure 17. The changes in the likelihoods near the peak (compared to using only the separation configuration probability) are small. If we understand the statistics for the incidence of gravitational lenses, then the lens redshifts provide some additional information but they do not dramatically improve the constraints on statistical models. The advantage of the lens redshifts is that they are subject to fewer systematic errors than the absolute incidence of lenses in surveys (Kochanek 1992a). The addition of more lens redshifts will have a similar effect to that produced by adding more lens separation configuration probabilities. The problem is that of the remaining Snapshot Survey lenses, only PG1115+080 is likely to have a measurable redshift—both 1413+117 and 1208+101 probably have lens galaxies that are too faint to measure their redshifts (Kochanek 1992a).

6.3. *Improving the Selection Function*

Surprisingly, the weakest part in the designs of the optical surveys is their choice of an outer survey radius. The outer radii of the Snapshot Survey, Crampton et al. (1992), and Yee et al. (1992) surveys are 7.″0, 6.″0, and 10.″0, respectively. The Snapshot Survey and

[4] To include the image separation configuration probability we needed only to assume that the selection function was uniform over the angular ranges in Table 2. The actual completeness did not matter.

Crampton et al. (1992) outer radii significantly weaken the constraints on large values of σ_* which leads to weaker constraints on cosmologies with low lensing optical depths. Since the spirit of our approach to this problem is to measure parameters such as σ_* directly using lens statistics rather than using previously measured values, an increase of the outer survey radius will strengthen the constraints on large values of σ_* and low optical depth cosmologies. The advantage of this change is that it does not require a new survey of the quasars but only the identification of already discovered companions. The disadvantage is that the number of contaminating stars rises with an increase in the radius (Kochanek 1993b). The costs of following up all the candidates can be greatly reduced by using a selection function for the region outside 7".0 which cuts off only about 2 mag fainter than the quasar—this is enough to set a limit on the number of lenses without including many contaminating stars.

Another reason to expand the survey region is the existence of the large separation ambiguous lens candidates 2345 + 007, 1634+267, and 1120+019 (see Surdej et al. 1992a). We argued in Paper I that the large flux ratios typical of these systems are characteristic of associated quasar pairs and not gravitational lenses. If we can rule out the existence of any small flux ratio but large separation systems we will have very strong evidence that these systems are not lenses but associated quasars.

6.4. *Larger Lens Survey*

If we could simply double the size of the existing surveys we would convert the 30% likelihood contour in the existing likelihoods into 10% contours of the larger survey (if the statistical properties of the sample do not change). The problem with doubling the survey size is that we do not have another 500 bright quasars. As a result, almost any follow-up survey will tend to be fainter and hence have less magnification bias than the existing survey. On the other hand, the average redshift of the objects in a new survey may be higher, which will partially compensate for the reduced magnitudes. Since the differences between cosmologies tend to be larger at higher redshifts, this may increase the ability of the surveys to distinguish between cosmological models.

If the goal is simply to find new lenses, then we can estimate the number of quasars that must be examined to achieve a 90% Poisson probability (the expected number of lenses is 2.3) of finding a new lens assuming the existing statistical model is correct. For the best-fit Einstein-de Sitter model without 0957+561 ($\sigma_* = 245$ km s^{-1}) a survey must examine 440, 270, 190, or 160 quasars at 18 V magnitudes and redshifts of $z = 2$, 3, 4, and 5 to have a 90% probability of finding a new lens. If we examine quasars that are 19 V magnitudes or fainter, we must examine 1500, 900, 680, or 560 quasars at $z = 2$, 3, 4, and 5 to achieve the same goal.

If the goal is to differentiate between cosmological models, then the task is considerably harder. Since $\Omega_\Lambda \simeq 1$ is already ruled out, we can ask how many survey quasars are needed to produce a factor of 10 difference in the likelihoods between cosmologies with $\Omega_M = 1$ and $\Omega_M = 0$ when $\Omega_\Lambda = 0$. If we fix the value of σ_*, then most of the likelihood differences come from the number and distribution of the observed lenses. Suppose we are in a cosmology where the probability of lensing a quasar at a given quasar redshift and magnitude is p_1, and we are trying to rule out a cosmology with lensing probability p_2 for the same redshift and magnitude. The likelihood difference between the two models increases with the number of quasars sampled N as

$$\Delta \ln P = N\left(-p_1 + p_2 + p_1 \ln \frac{p_1}{p_2}\right). \tag{6.1}$$

If our condition for ruling out a cosmological model is that its likelihood is 10 times lower than the peak, then we must survey enough quasars to reach $\Delta \ln P = 2.3$. This condition is a lower limit on the required number because we fixed σ_*—if the velocity dispersion scale varies between the two cosmologies it can partially compensate for the differences in optical depth. If we apply this condition to differentiating between the Einstein-de Sitter cosmology and an empty cosmology, we need 1800, 800, 500, 300 $m_V = 18$ quasars at redshifts of $z = 2$, 3, 4, and 5 respectively, and 6300, 2700, 1600, or 1100 $m_V \geq 19$ quasars. A much larger survey is needed to differentiate between these two cosmologies than is needed to find a new lens. The existing optical sample of 600 objects roughly matches the probabilities for $z = 2$ and $m = 18$, so the probability difference between these two cosmologies is about a factor of 2.

7. SUMMARY

The statistics of the Snapshot Survey, Crampton et al. (1992), and Yee et al. (1992) surveys combined with the lenses found in the radio surveys (Burke et al. 1992; Patnaik et al. 1992a, b, c) are statistically consistent with a standard distribution of galaxies modeled as singular isothermal spheres in a standard Einstein-de Sitter cosmology. No variation of any input parameter examined in this paper leads to a statistically significant improvement in the likelihoods.

1. There is no $(3/2)^{1/2}$ correction to the velocity dispersions of E/S0 galaxies in the singular isothermal sphere model of gravitational lenses. If we use the Jeans equations, realistic density distributions like the Hernquist (1990) or Jaffe (1983) models, and observed radial velocity dispersion profiles, the best estimate of the isothermal sphere velocity dispersion is $\sigma_{DM} \simeq 0.9$–$1.1 v_c$, where v_c is the observed velocity dispersion. The estimated velocity dispersion scale of L_* E/S0 galaxies is $\sigma_* \simeq 215$ km s^{-1} with an allowed range approximately 183 km s^{-1}–248 km s^{-1}. The addition of a small core radius to the isothermal model can raise the estimated velocity dispersion by 5–10% without significantly altering the lensing properties.

2. The size distribution of the known gravitational lenses determines the mass scale of galaxies nearly as well as dynamical studies. In an Einstein-de Sitter cosmology, the 90% confidence interval for the velocity dispersion of an L_* E/S0 galaxy is 210 km s^{-1} $\lesssim \sigma_* \lesssim$ 270 km s^{-1} with a best-fit value of 245 km s^{-1} excluding the systematic uncertainties from the treatment of the lens 0957+561. This is consistent with the dynamical estimates. Doubling the survey size will reduce the confidence limits by 10–20 km s^{-1} at both ends and make gravitational lens statistics a strong, direct competitor with dynamics of individual galaxies. The limits on large velocity dispersions are weakened by the small areas searched around each quasar for lensed images.

3. Gravitational lenses do not favor a large cosmological constant, but the limits are much weaker than suggested by studies that use fixed values for σ_* and the Gott (1977) $(3/2)^{1/2}$ correction to the velocity dispersions. If we exclude 0957+561 and assume spiral galaxies are subcritical, then the upper limit is $\Omega_\Lambda \lesssim 0.8$ with 90% confidence, and at this limit $\sigma_* = 200$ km s^{-1}.

4. There is no statistical evidence for or against a contribution by spiral galaxies to gravitational lensing. The low-velocity dispersion of the spirals and the small number of lenses makes it impossible to detect or reject a contribution from spiral galaxies in the current surveys. The contribution from spiral galaxies reduces the limit on a cosmological constant to $\Omega_\Lambda \lesssim 0.6$ because the spiral galaxies become very important for larger Ω_Λ and $\sigma_* \simeq 200$ km s^{-1}.

5. There is no statistical evidence for the presence of dark galactic halos that can produce multiple images. The estimated density of E/S0 galaxies using lens statistics agrees with direct determinations remarkably well, although the 90% confidence level errors are substantially larger. The 90% confidence level upper limit on the density of mass concentrations with E/S0 masses in an Einstein-de Sitter cosmology is $0.017h^3$ Mpc^{-3}, compared to the observed density of $5 \times 10^{-3}h^3$ Mpc^{-3}.

6. Gravitational lenses cannot, as yet, determine the parameters of the Schechter function on the "Tully-Fisher" relation with any great accuracy, but the results are consistent with standard observational results. The best-fit value for the Schechter function exponent is $\alpha = -1.15$ and the best-fit values for the Tully-Fisher exponent are $\gamma = 3.7$ ($\gamma = 4.7$) with (without) 0957+561. The constraints on the exponent of the Schechter function are weak because there are two values of α at which a Schechter distribution can produce the same mean image separation and expected number of lenses. Doubling the survey size will substantially reduce the uncertainties, although they will still be somewhat larger than those from conventional methods. Much of the uncertainty is caused by the weak limits on large velocity dispersion lenses arising from the small outer survey radius of 7".0 used by the Snapshot Survey.

7. All the large discrepancies between the standard parameters and the maximum likelihood solutions are associated with the variables that control the magnification bias, particularly the faint end slope of the quasar number counts, β, and the minimum magnification produced by the lenses, M_0. None of the deviations are statistically significant (defined by the 90% confidence level), and they are larger when we include 0957+561 than when we exclude it. The lenses found by the optical surveys hug the very bright edge of the distribution of the survey quasars, and they are somewhat brighter than typical samples of lenses generated from Monte Carlo experiments. We know that we have underestimated the typical magnification, because of the presence of the four image lenses PG1115+080 and 1413+117. The four image lenses have much larger mean magnifications ($M_0 \sim \epsilon^{-1}$ where $\epsilon \sim 0.1$ is the ellipticity) than the three image lenses, but they also have a much smaller cross section. The SIS model can only partly mimic this effect by raising M_0 and reducing σ_* because a reduction in σ_* also alters the separation distribution. These points suggst that the statistics are sensitive to the presence of ellipticity in the lens model (beyond the simple appearance of four image lenses) through the magnification probability distribution. Experiments to determine ϵ were swamped by the Poisson errors arising from the small numbers of lenses. Lens statistics are not consistent with the quasar number counts model of Hawkins & Véron (1993). Their number counts have no break near 19 B mag, which removes the differential magnification bias for bright and faint quasars seen in the lens surveys.

8. The method used to find the quasar has no detectable effect on the likelihood that the quasar is lensed. If the selection technique has no effect on the lens statistics we expect that 26%, 11%, 60%, and 3% of the lenses in the Snapshot Survey would be quasars found by radio surveys, color selection, spectral methods, or other methods. The observed sample has one radio-selected quasar (0957+561), one color-selected quasar (PG1115+080), and three spectrally selected quasars (0142−100, 1208+101, 1413+117). The distribution (20%, 20%, 60%, 0%) is statistically indistinguishable from the predicted distribution if the selection technique had no effect on the lens statistics. The selection effects for optically selected quasars discussed by Kochanek (1991b) would not be detectable in such a small sample, because the typical magnitude of the effects were only 10%–30% for $m \lesssim 19$ B mags. There is no evidence for "double magnification bias" (Borgeest, Linde, & Refsdal 1991) in the sample. If radio and optical fluxes are uncorrelated then a sample first selected for being a bright radio source, and then selected for being a bright optical source would gain from two independent magnification biases for the two steps in the selection process. There is no evidence for such an effect in the Snapshot Survey.

The author thanks Ramesh Narayan for discussions about this work and the persistence of an anonymous referee. This research was supported by an Alfred P. Sloan Foundation Fellowship.

REFERENCES

Bahcall, J. N., Maoz, D., Doxsey, R., Schneider, D. P., Bahcall, N. A., Lahav, O., & Yanny, B. 1992, ApJ, 387, 56
Blandford, R. D., & Kochanek, C. S. 1987, ApJ, 321, 658
Borgeest, U., Linde, J. V., & Refsdal, S. 1991, A&A, 251, L35
Burke, B. F., Lehàr, J., & Connor, S. R. 1992, in Gravitational Lenses, ed. R. Kayser, T. Schramm, & L. Nieser (Berlin: Springer), 237
Crampton, D., McClure, R. D., & Fletcher, J. M. 1992, ApJ, 392, 23
de Vaucouleurs, G. 1948, Ann. d'Ap., 11, 247
de Vaucouleurs, G., & Olson, D. W. 1982, ApJ, 256, 346
Efstathiou, G., Ellis, R. S., & Peterson, B. A. 1988, MNRAS, 232, 431
Faber, S. M., & Jackson, R. E. 1976, ApJ, 204, 668
Fukugita, M., & Turner, E. L. 1991, MNRAS, 253, 99
Gott, J. R. 1977, ARA&A, 15, 235
Gott, J. R., & Gunn, J. E. 1974, ApJ, 190, L105
Hartwick, F. D. A., & Schade, D. 1990, ARA&A, 28, 437
Hawkins, M. R. S., & Véron, P. 1993, MNRAS, 260, 202
Hernquist, L. 1990, ApJ, 356, 359
Huchra, J., Gorenstein, M., Kent, S., Shapiro, I., Smith, G., Horine, E., & Perley, R. 1985, AJ, 90, 691
Jaffe, W. 1983, MNRAS, 202, 995
Kaiser, N., & Tribble, P. 1991, in The Space Distribution of Quasars, ed. D. Crampton, ASP Conference Series 21 (ASP: San Francisco), 304
Kochanek, C. S. 1991a, ApJ, 373, 354
———. 1991b, ApJ, 379, 517
Kochanek, C. S. 1992a, ApJ, 348, 1
———. 1992b, ApJ, 397, 381
———. 1993a, MNRAS, 261, 453
———. 1993b, ApJ, 417, 438
Kochanek, C. S., & Blandford, R. D. 1987, ApJ, 321, 676
Kochanek, C. S., & Lawrence, C. R. 1990, AJ, 99, 1700
Krauss, L. M., & White, M. 1992, ApJ, 394, 385
Lehàr, J. 1992, Ph.D. thesis, MIT
Lupton, R. L. 1993, Statistics in Theory and Practice (Princeton Univ. Press: Princeton)
Maoz, D., Bahcall, J. N., Doxsey, R., Schneider, D. P., Bahcall, N. A., Lahav, O., & Yanny, B. 1993a, ApJ, 402, 69
Maoz, D., Bahcall, J. N., Schneider, D. P., Doxsey, R., Bahcall, N. A., Fillipenko, A. V., Goss, W. M., Lahav, O., & Yanny, B. 1992a, ApJ, 386, L1
Maoz, D., Bahcall, J. N., Schneider, D. P., Doxsey, R., Bahcall, N. A., Lahav, O., & Yanny, B. 1992b, ApJ, 394, 51
Maoz, D., Bahcall, J. N., Schneider, D. P., Bahcall, N. A., Lahav, O., Djorgovski, S., Doxsey, R., Gould, A., Kirhakos, S., & Yanny, B. 1993b, ApJ, 409, 28
Magain, P., Surdej, J., Vanderriest, C., Pirenne, B., & Hutsemékers, D. 1992, A&A, 253, L13
Patnaik, A. R., Browne, I. W. A., King, L. J., Muxlow, T. W. B., Walsh, D., & Wilkinson, P. N. 1992a, in Gravitational Lenses, ed. R. Kayser, T. Schramm, & L. Nieser (Berlin: Springer), 140

Patnaik, A. R., Browne, I. W. A., King, L. J., Muxlow, T. W. B., Walsh, D., & Wilkinson, P. N. 1992b, MNRAS, in press
Patnaik, A. R., Brown, I. W. A., Walsh, D., Chaffee, F. H., & Foltz, C. B. 1992c, MNRAS, 259, 1P
Postman, M., & Geller, M. J. 1984, ApJ, 281, 95
Schechter, P. 1976, ApJ, 203, 297
Surdej, J., Claeskens, J. F., Crampton, D., Fillipenko, A. V., Hutsemékers, D., Magain, P., Pirenne, B., Vanderriest, C., & Yee, H. K. C. 1993, AJ, 105, 2064
Surdej, J., Claeskens, J. F., Hutsemékers, D., Magain, P., & Pirenne, B. 1992, in Gravitational Lenses, ed. R. Kayser, T. Schramm, & L. Nieser (Berlin: Springer), 27
Surdej, J., Magain, P., Swings, J.-P., Borgeest, U., Courvoisier, T. J.-L., Kayser, R., Kellerman, K. I., Kühr, H., & Refsdal, S. 1988, A&A, 198, 49
Tonry, J. L. 1983, ApJ, 266, 58
Tully, R. B., & Fisher, J. R. 1977, A&A, 54, 661
Turner, E. L. 1980, ApJ, 242, L135
———. 1990, ApJ, 365, L43
Turner, E. L., Ostriker, J. P., & Gott, J. R. 1984, ApJ, 284, 1
van der Marel, R. P. 1991, MNRAS, 253, 710
Wallington, S., & Narayan, R. 1993, ApJ, 403, 517
Yee, H. K. C., Fillipenko, A. V., & Tang, D. 1993, AJ, 105, 7
Young, P., Gunn, J. E., Kristian, J., Oke, J. B., & Westphal, J. A. 1980, ApJ, 241, 507